SCIENCE CHINA
Earth Sciences

• RESEARCH PAPER •

doi: 10.1007/s11430-016-9082-5

# High-pressure experimental verification of rutile-ilmenite oxybarometer: Implications for the redox state of the subduction zone

TAO RenBiao[1*], ZHANG LiFei[1], Vincenzo STAGNO[2], CHU Xu[3] & LIU Xi[1]

[1] *The Key Laboratory of Orogenic Belt and Crustal Evolution, School of Earth and Space Sciences, Peking University, Beijing 100871, China;*
[2] *Earth Sciences Department, Sapienza University of Rome, Rome 00185, Italy;*
[3] *Department of Geology and Geophysics, Yale University, New Haven, Connecticut 06520, USA*

Received November 10, 2016; accepted July 4, 2017; published online August 22, 2017

**Abstract** The more oxidized mantle peridotites above subducting slabs than stable continental areas have been attributed to the infiltration of some oxidizing fluids released from the subducting slabs. However, knowledge for the redox states of the slabs itself is very limited. Until now, few oxybarometers can be directly used to constrain the redox states of the subducting slabs. The rutile-ilmenite oxybarometer was proposed and successfully applied to constrain the oxygen fugacity of mantle assemblages. However, its application to rocks equilibrated at crustal *P-T* conditions has been hampered by some uncertainties in an early solid solution model of ilmenite. With a newly-released solid solution model for the ilmenite, we have conducted high-P experiments (at 3 and 5 GPa, and 900–1300°C) to test the accuracy of this oxybarometer. The experiments were performed with their oxygen fugacities controlled by the CCO buffer (i.e., $C+O_2=CO_2$). We demonstrated that the oxygen fugacities calculated for our high-P experimental products by using the rutile-ilmenite oxybarometer were in excellent agreement with the $fO_2$ dictated by the CCO buffer, suggesting a wide applicability of this oxybarometer to crust rocks. As examples, the rutile-ilmenite oxybarometer has been used to constrain the oxygen fugacities of some metamorphic rocks such as eclogite, granulite and amphibolite usually observed from the subduction zones.

**Keywords** High-pressure experiment, Ilmenite-rutile oxybarometer, Oxygen fugacity, Subduction zone

**Citation:** Tao R B, Zhang L F, Stagno V, Chu X, Liu X. 2017. High-pressure experimental verification of rutile-ilmenite oxybarometer: Implications for the redox state of the subduction zone. Science China Earth Sciences, doi: 10.1007/s11430-016-9082-5

## 1. Introduction

Oxygen fugacity ($fO_2$) is one of the most important parameters in determining the relative stability of oxides, sulfides, silicates and carbonates in both igneous and metamorphic rocks (Lindsley, 1991). It also has significant effect on some chemical (i.e. solidus, liquidus and elemental partitioning) and physical properties (i.e. creep and electrical conductivity) of these rocks (Arculus, 1985; Ryerson et al., 1989; Dai et al., 2014). Numerous methods thus have been developed and applied to constrain the redox state of these rocks (Christie et al., 1986; Wood and Virgo, 1989; Parkinson and Arculus, 1999; Bézos and Humler, 2005; Canil and Bellis, 2007; Bellis and Canil, 2006; Lee et al., 2010). Peridotites from the mantle wedges above subducting slabs, with their $fO_2$ ranging from ~FMQ to ~FMQ+2 (commonly>~FMQ+1), are more oxidized than those from the stable continental areas (Frost and McCammon, 2008; Foley, 2011). This more oxidized state is usually attributed to the addition of some very oxidizing agent of fluids or melts from the subducting slabs (Parkinson and Arculus, 1999; Wood and Virgo, 1989; Bézos and Humler, 2005; Malaspina et al., 2009; Kelley and Cottrell, 2009). However, very few oxybarometers have been actually used to

* Corresponding author (email: rbtao@pku.edu.cn)

constrain the $fO_2$ of the subducting crustal rocks, mainly because of the low temperatures and the complicated $fO_2$ evolution of the rocks in the subduction zones (Foley, 2011).

Based on some special mineral assemblages (e.g. almandine+$O_2$=magnetite+sillimante+quarts) (Anovitz et al., 1993), some oxybarometers have been proposed to estimate the $fO_2$ of some crustal rocks in some special system (e.g. metamorphosed iron formations) (Frost, 1979a, 1979b). Since these phase assemblages are not commonly found in the metamorphic crustal rocks from the subduction zones, these oxybarometers are of limited use.

Fe-Ti oxides are important indicators of $fO_2$, and may be sensitive monitors to the redox state of the metamorphic rocks in the subduction zones where some of the $Fe_2O_3$-$FeTiO_3$, $Fe_3O_4$-$Fe_2TiO_4$, $Fe_2TiO_5$-$FeTi_2O_5$ and $Fe_{1-x}O$-$TiO_2$ pairs are often found (Buddington and Lindsley, 1964; Lindsley, 1991; Liou et al., 1998) (Figure 1). The phase assemblages of hematite+ilmenite and magnetite+ulvöspinel have been calibrated as oxybarometer and thermometer (Buddington and Lindsley, 1964; Ghiorso, 1990; Ghiorso and Evans, 2008), and successfully applied to some igneous rocks (Lindsley, 1991). However, they are less well suited for the low to medium grade metamorphic rocks because of the limited solid solution behavior between the magnetite and ulvöspinel, and between the hematite and ilmenite at low temperatures (Ghiorso, 1990; Donohue and Essene, 2000). The rutile-ilmenite oxybarometer is based on the reaction and has been applied to igneous rocks (Carmichael and Nicholls, 1967) and ilmenite-bearing mantle assemblages (Zhao et al., 1999). However, the application of this oxybarometer to the rocks equilibrated at crustal *P-T* conditions has been hampered by the large uncertainties in the mixing behavior between ilmenite and hematite (Ghiorso, 1990; Andersen et al., 1991). Recently Ghiorso and Evans (2008) developed a new model for the thermodynamic properties of the ilmenite solid solutions in the system $Fe_2O_3$-$FeTiO_3$-$MgTiO_3$-$MnTiO_3$ with or without minor $Al_2O_3$. This model accounts for the temperature and compositional dependences of the long-range cation-order and the related high- to low-symmetry structural phase transition. It has been successfully applied to the two-oxide geo-thermometer/oxygen barometer for igneous rocks and mantle xenoliths (Ghiorso and Evans, 2008). Since the rutile-ilmenite assemblages are ubiquitous in eclogites, granulites and amphibolites from subduction zones (Liou et al., 1998), it is interest to integrate the rutile-ilmenite oxybarometer (Carmichael and Nicholls, 1967) with this new ilmenite solid solution model, which may lead to an accurate oxybarometer applicable to the metamorphic rocks formed at the crust *P-T* conditions.

$$4\mathrm{FeTiO_3(inilmenite)} + \mathrm{O_2} = 2\mathrm{Fe_2O_3(inilmenite)} + 4\mathrm{TiO_2(inrutile)}. \quad (1)$$

In this study, we carried out a series of high-pressure experiments in the system FeO-$TiO_2$-$CO_2$ under $fO_2$ controlled by the CCO buffer (the reaction C+$O_2$=$CO_2$) to verify if the rutile-ilmenite oxybarometer, with the new ilmenite solid solution model, could correctly reproduce the $fO_2$ in the experiments.

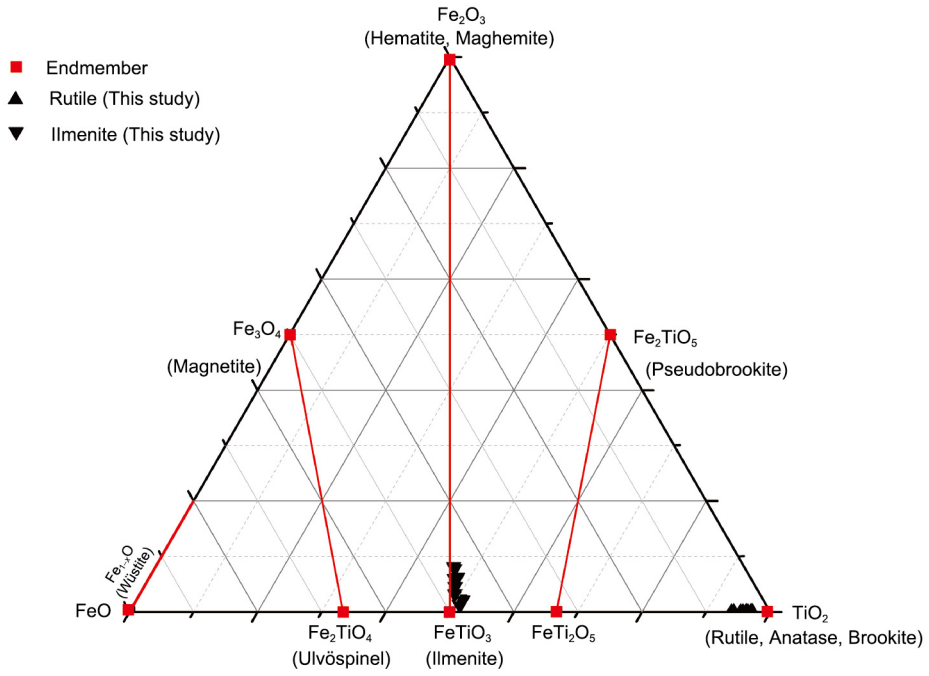


**Figure 1** Phases in the system FeO-$Fe_2O_3$-$TiO_2$ modified after Buddington and Lindsley (1964), showing the major solid solution series (red lines) of $Fe_3O_4$-$Fe_2TiO_4$, $Fe_2O_3$-$FeTiO_3$, and $Fe_2TiO_5$-$FeTi_2O_5$. Red solid squares represent possible end-members in the system; black solid triangles represent chemical composition of rutile and ilmenite from high-pressure experiments in this study.

## 2. Experimental methods

Experiments in the system FeO-$TiO_2$-$CO_2$ were conducted at pressures of 3–5 GPa and temperatures of 900–1300°C at the High-Pressure and High-Temperature Laboratory of Peking University. The starting material consisted of natural siderite ($FeCO_3$) (Ivigtut, Greenland) and chemical reagent $TiO_2$ (99.995%, Alfa Aesar). The composition of the siderite, determined with a JEOL 8900 microprobe at the Geophysical Laboratory of Carnegie institution of Washington, is $(Fe_{0.950}Mn_{0.046}Mg_{0.004})CO_3$, indicating that the siderite is almost a pure end-member. The effect of the minor Mg and Mn in the siderite on the thermodynamic properties of ilmenite can be well accounted for by the new solid solution model of ilmenite (Ghiorso and Evans, 2008). The mole ratio of $TiO_2$ to siderite in the starting material was over 1:1. The mixed starting material was ground under ethanol in an agate mortar. No wüstite but siderite was used as the FeO source in the starting material, so as to generate some $CO_2$ (Tao et al., 2013) for the CCO buffer together with the graphite capsule. All of the experiments at 3 and 5 GPa were carried out on a large cubic press with a maximum load of 1400 tons on every WC anvil (Liu et al., 2012). Temperatures were measured with a B-type thermocouple ($Pt_{94}$-$Rh_6$/$Pt_{70}$-$Rh_{30}$) positioned at the center of the graphite furnace. Details on the cell assembly (BJC-11) and its pressure calibrations were described previously (He et al., 2014). The temperature gradient across the 2.5-mm-long graphite capsule was <25°C (Liu et al., 2012). Both pressures and temperatures were automatically controlled during the whole experimental process. The experiments were first pressurized to the desired pressures, then heated up at a rate of 100°C $min^{-1}$, and finally held at constant target temperatures for sufficient durations to closely approach their equilibrium. They were quenched by shutting off the power supply to the furnace, and automatically decompressed to atmospheric pressure at a rate of −1 GPa $h^{-1}$.

After the experiments, each run product was cut into two parts with a diamond saw. One part of the sample was mounted on a glass fiber for collecting X-ray diffraction (XRD) pattern. The XRD pattern was collected with a SMART APEX-CCD X-ray diffractometer at the China University of Geoscience (Beijing). This instrument was operated at 40 kV and 30 mA, and with a Mo K-alpha radiation. The derived XRD pattern was analyzed by the Jade 6.0 software, and compared with the relevant PDF cards in order to identify the phases. The other part of the sample was mounted in epoxy resin, polished with aluminum oxide powder, and analyzed by using a scanning electron microscope (SEM; Quanta™ 650 FEG) and an electron microprobe at Peking University (EMP; JEOL JXA-8800R).

## 3. Experimental results

### 3.1 Phase relations

In total, 8 high-pressure experiments were carried out under their $fO_2$ controlled with the CCO buffer. The experimental conditions and run products are listed in Table 1. At each pressure, 4 experiments were carried out to constrain the effect of temperature on the stability of rutile+ilmenite assemblage. According to previous experimental results (Tao et al., 2013), all of the experimental conditions were near the decomposition boundary of siderite. At relatively low temperatures, siderite was still a stable phase, and the phase assemblage siderite+rutile+ilmenite was observed, which indicated partial breakdown of the siderite. At relatively high temperatures, siderite was not stable any more, and ilmenite was the only crystalline phase coexisting with rutile in the run products (Table 1).

At 3 GPa and 900°C, and with a heating duration of 48 hours (SR-4), siderite was still observed in equilibrium with rutile and ilmenite. On the XRD pattern, strong ilmenite peaks have been identified, with medium rutile peaks and weak siderite peaks observed (Figure 2). With temperature increased to 950°C and a heating duration of 36 hours (SR-7), rutile and ilmenite were the only phases in equilibrium, as indicated by the XRD pattern (Figure 2). When the experimental charge was heated for 24 h at 1000°C (SR-1), only a small amount of rutile was sporadically distributed in the major

**Table 1** Experimental conditions and run products[a)]

| Sample | *P* (GPa) | *T* (°C) | Time (h) | Run products |
|---|---|---|---|---|
| SR-4 | 3 | 900 | 36 | Sd+Ru+Ilm |
| SR-7 | 3 | 950 | 48 | Ilm+Ru |
| SR-1 | 3 | 1000 | 24 | Ilm+Ru |
| SR-2 | 3 | 1200 | 24 | Ilm+Ru+Melt |
| SR-5 | 5 | 1100 | 24 | Sd+Ru+Ilm |
| SR-6 | 5 | 1150 | 24 | Sd+Ru+Ilm |
| SR-3 | 5 | 1200 | 24 | Ilm+Ru |
| SR-8 | 5 | 1300 | 24 | Ilm+Ru+Melt |

a) Sd: siderite; Ru: rutile; Ilm: ilmenite; Melt: liquid phase

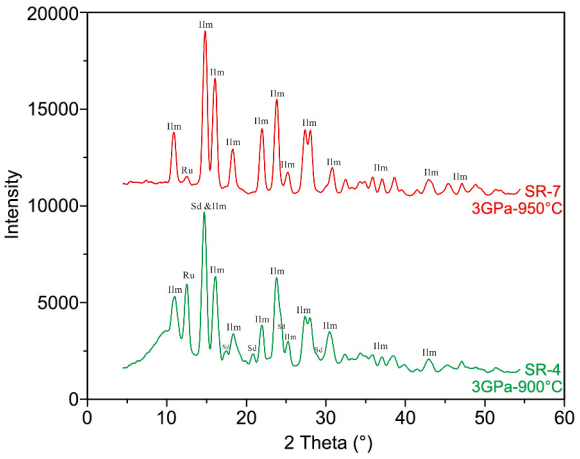


**Figure 2** Selected XRD patterns of run products at 3 GPa. Typical diffraction peaks of the major phases are marked on XRD patters.

phase of ilmenite, as illustrated by the BSE image (Figure 3a). In the experiment at still higher temperature (SR-2: 1200°C, 24 h), melt was observed in equilibrium with residual rutile and ilmenite (Figure 3b).

When pressure increased to 5 GPa, a large amount of siderite was observed in the experiments at 1100°C (SR-5) and 1150°C (SR-6) (Figure 3c), suggesting that these *P-T* conditions were still in the stable field of siderite (Tao et al., 2013). We observed the subsolidus phase assemblage rutile+ilmenite at 1200°C (SR-7; Figure 3d), and the melt-bearing phase assemblage melt+rutile+ilmenite at 1300°C (SR-8).

In summary, rutile and ilmenite coexisted in all experimental runs (Table 1), with either a small amount of siderite present in the experiments at relatively low temperatures (SR-4, SR-5 and SR-6) or a small amount of melt present in the experiments at relatively high temperatures (SR-2 and SR-8). As suggested by the large grain sizes of the coexisting phases, their clear phase boundaries, and their chemical compositions collected by the EMP (to be discussed below), these experiments have attained close equilibrium, and can be used to verify the rutile-ilmenite oxybarometer for the *P-T* range covered by the high-*P* experiments.

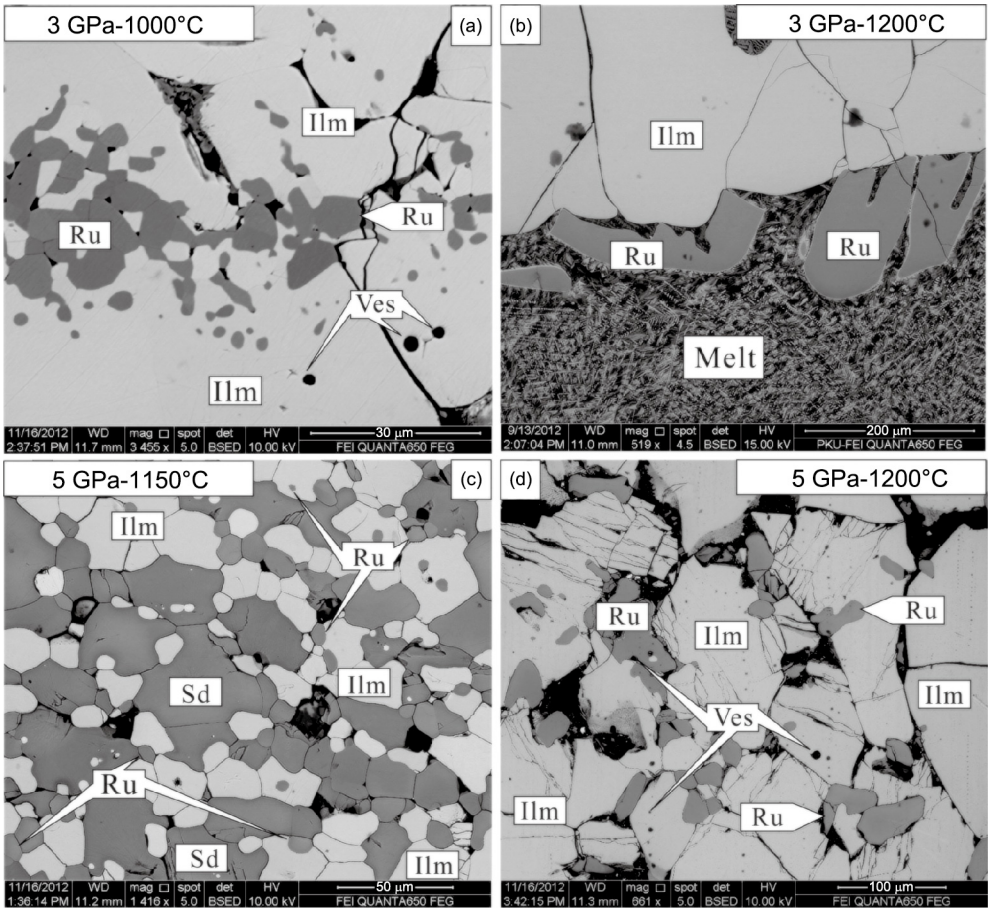


**Figure 3** BSE images of representative run products, with experimental conditions marked on the images. (a) Run SR-1: Small rutile (Ru) grains distributed in large ilmenite (Ilm) grains, gas vesicles (Ves) are present in the run products. (b) Run SR-2: Large ilmenite grains with small amounts of rutile in equilibrium with melt. (c) Run SR-6: Coexisting siderite, rutile and ilmenite grains. (d) Run SR-3: Coexisting rutile and ilmenite. Gas vesicles are present in all the run products. Abbreviations: Ilm=ilmenite; Ru=rutile; Sd=siderite; Melt=melt. The mineral abbreviation followed Whitney and Evans (2010) in all tables and figures.

### 3.2 $fO_2$

Some special experimental techniques such as the double-capsule method have been developed for the piston-cylinder apparatus (Jakobsson, 2012), which is typically for high-*P* experiments up to about 3 GPa. For the high-*P* experiments at still higher pressures, either a cubic press or a multi-anvil press has to be in place. Due to the limited sample volume in both types of the high-*P* press, it is often difficult to carry out experiments with their $fO_2$ well-controlled. Here we took advantage of the massive size of our cubic press (Liu et al., 2012), and conducted some experiments with well-controlled $fO_2$ at 3 and 5 GPa.

In order to control the oxygen fugacity in our experiments with the CCO buffer, we used the graphite capsule and siderite to provide both C and $CO_2$, respectively. According to Tao et al. (2013), the stability of siderite is partially controlled by the oxygen fugacity and carbon dioxide fugacity, and its decomposition products vary a lot under different experimental conditions. At the beginning of the decomposition, siderite will decompose to FeO and $CO_2$ (French and Rosenberg, 1965). In our experiments, some FeO product would further react with the $TiO_2$ to form the $FeTiO_3$ whereas the released $CO_2$ gas and graphite capsule would buffer the whole experimental charge at the $fO_2$ level of the CCO buffer. This has been verified by the presence of gas vesicles in the experimental charges (Figure 3). The $CO_2$ should be the dominanet carbon oxide species in the run products because high-pressure would have driven CO into the stable phase assemblage of graphite+$CO_2$ via the Boudouard reaction (Tao et al., 2013):

$$2\mathrm{CO} = \mathrm{CO_2} + \mathrm{C}. \quad (2)$$

So the activity of the $CO_2$ and C in the products should be ~1, and the $fO_2$ of the experiments should be well buffered by CCO buffer.

Further, some FeO produced by the breakdown reaction of the siderite would have been oxidized as $Fe_2O_3$, which would enter the structure of the $FeTiO_3$. This solid solution behavior provides a redox indicator for the experimental charges based on the RI oxygen buffer (reaction 1).

### 3.3 Verification of $fO_2$

In order to apply the rutile-ilmenite (RI) oxybarometer (eq. (1)), we need to know the activity of $FeTiO_3$ and $Fe_2O_3$ in ilmenite, and the activity of $TiO_2$ in rutile. With the new solid solution model of ilmenite derived by Ghiorso and Evans (2008), the activities of $FeTiO_3$ and $Fe_2O_3$ in ilmenite have been calculated from the EMP compositional data (Tables S1 (http://link.springer.com) and Table 2). The activity of $TiO_2$ in rutile was simply replaced by the mole fraction of $TiO_2$ in rutile (Table 2), as suggested by Zhao et al. (1999).

The $fO_2$ of our experiments have been calculated by the equation from Zhao et al. (1999):

$$\begin{aligned}\log f\mathrm{O_2} = {} & 22.59 - 25925/T - 3.09\log T + 0.0016535P \\ & + 48.836P/T - 4\log\alpha\mathrm{IlmFeTiO_3} \\ & + 2\log\alpha\mathrm{IlmFe_2O_3} + 4\log\alpha\mathrm{RutTiO_2}. \end{aligned} \quad (3)$$

where *T* is in kelvin and *P* is in kbar (Table 2). The derived $fO_2$ values are listed in Table 2, and plotted in Figure 4.

Alternatively, our experiments were fully controlled by the CCO buffer, so that their $fO_2$ could be straightforwardly calculated. In this calculation, we used the ThermoCalc Software (tc336i) with the newly updated thermodynamic data of Holland and Powell (2011). The results from this calculation are shown in Figure 4. Figure 4 clearly shows that the $fO_2$ values calculated with the rutile-ilmenite oxybarometer are in excellent agreement with the CCO buffer. This agreement strongly argues for the application of the rutile-ilmenite oxybarometer to these crust rocks. As expected, the presence of extra coexisting phases such as siderite and melt does not affect the applicability of the rutile-ilmenite oxybarometer.

## 4. Application of the ilmenite-rutile oxybarometer

Rutile and ilmenite coexist ubiquitously in some metamor-

**Table 2** Phase composition and $fO_2$ of experiments calculated by RI oxybarometer[a)]

| No. | *P* (GPa) | *T* (K) | Mole fractions | | | | | Activity | | | | | log$fO_2$ |
|---|---|---|---|---|---|---|---|---|---|---|---|---|---|
| | | | $FeTiO_3$ | $MgTiO_3$ | $MnTiO_3$ | $Fe_2O_3$ | $TiO_2$ | $Fe_2O_3$ | $FeTiO_3$ | $MgTiO_3$ | $MnTiO_3$ | $TiO_2$ | RI |
| SR-4 | 3 | 1173 | 0.90(5) | 0.00(0) | 0.03(1) | 0.06(4) | 0.96(6) | 0.05(1) | 0.88(4) | 0.00(0) | 0.01(5) | 0.96(6) | −10.124 |
| SR-7 | 3 | 1223 | 0.88(5) | 0.01(1) | 0.05(0) | 0.04(6) | 0.96(8) | 0.03(4) | 0.86(6) | 0.02(0) | 0.02(6) | 0.96(8) | −9.648 |
| SR-1 | 3 | 1273 | 0.90(2) | 0.00(6) | 0.04(6) | 0.04(1) | 0.97(1) | 0.02(4) | 0.88(3) | 0.01(1) | 0.02(3) | 0.97(1) | −9.255 |
| SR-2 | 3 | 1473 | 0.88(1) | 0.0(4) | 0.03(7) | 0.04(2) | 0.97(3) | 0.01(2) | 0.85(8) | 0.05(9) | 0.01(7) | 0.97(3) | −7.399 |
| SR-5 | 5 | 1373 | 0.86(0) | 0.00(2) | 0.02(6) | 0.11(3) | 0.95(8) | 0.05(6) | 0.84(3) | 0.00(4) | 0.01(0) | 0.95(8) | −6.401 |
| SR-6 | 5 | 1423 | 0.82(6) | 0.00(2) | 0.02(5) | 0.14(4) | 0.94(3) | 0.06(0) | 0.81(3) | 0.00(4) | 0.00(9) | 0.94(3) | −5.752 |
| SR-3 | 5 | 1473 | 0.84(2) | 0.00(3) | 0.03(9) | 0.11(4) | 0.96(4) | 0.04(2) | 0.81(5) | 0.00(6) | 0.01(4) | 0.96(4) | −5.524 |
| SR-8 | 5 | 1573 | 0.88(2) | 0.00(5) | 0.02(7) | 0.08(7) | 0.94(8) | 0.02(2) | 0.83(7) | 0.00(9) | 0.00(9) | 0.94(8) | −4.923 |

a) The errors in parentheses are standard derivations of multiple analyses (5–8 measurements for each mineral phases). The original EMP data are listed in Table S1

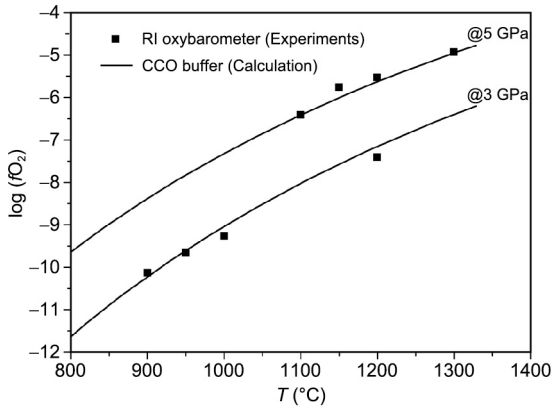


**Figure 4** Log($fO_2$)-$T$ diagram. Solid lines are thermodynamically calculated for the CCO buffer at 3 and 5 GPa using the ThermoCalc program. Solid squares stand for the calculated $fO_2$ of our experiments using the rutile-ilmenite oxybarometer (eq. (3)), which incorporated the new solid solution model of ilmenite.

phic rocks such as eclogites, granulites, and amphibolites from different subduction zones (Liou et al., 1998). With the above verification, we can therefore use the rutile-ilmenite oxybarometer to constrain the $fO_2$ of these metamorphic rocks.

We have applied the rutile-ilmenite oxybarometer to an eclogite from Southwestern Tianshan, China (Tao et al., 2014), an eclogites from Songduo, Tibet, China (Yang et al., 2014), a granulites from Tongbai, Dabie Shan, China (Bader et al., 2014), and a amphibolite from Wutai-Hengshan, North China (Qian and Wei, 2016). The coexistence of rutile and ilmenite assemblage in these rocks is shown in Figure 5.

The $P$-$T$ evolution paths of these rocks were previously constrained by thermodynamic calculations and petrographic studies (Tian and Wei, 2013; Yang et al., 2014; Bader et al., 2014; Qian and Wei, 2016), and are summaried in Figure 6. Additionally, we have plotted in Figure 6 the different metamorphic facies for the composition system of MORB+$H_2O$ (Liou et al., 2004), and the experimentally-determined $P$-$T$ boundaries separating the rutile, titanite and ilmenite stability fields in the MORB+$H_2O$ system (Liou et al., 1998). For the MORB bulk-rock composition, rutile occupies a broad $P$-$T$

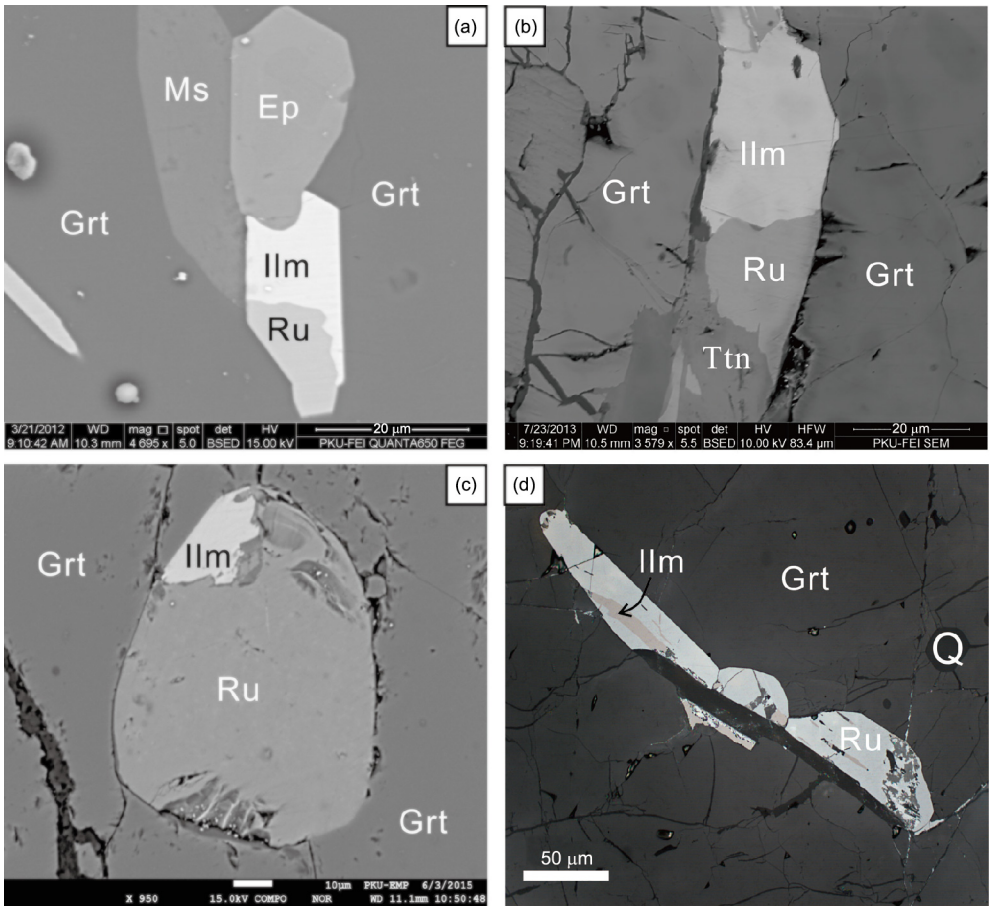


**Figure 5** Coexisting rutile and ilmenite in different metamorphic rocks. (a) BSE image of coexisting rutile (Ru) and ilmenite (Ilm), along with epidote (Ep) and muscovite (Ms), occurring as mineral inclusions in garnet (Grt) (eclogite A300-9; Southwestern Tianshan). (b) BSE image of coexisting rutile and ilmenite, along with titanite, occurring as mineral inclusions in garnet (eclogite SD-30; Sundo, Lhasa block of Tibetan Plateau). (c) BSE image of coexisting rutile and ilmenite garnet, occurring as mineral inclusions in garnet (amphibolite H1313; Hengshan, North China). (d) Polarizing microscopic photo of coexisting rutile and ilmenite, occurring as mineral inclusions in garnet (granulite 811133Y; Tongbai, Dabie).

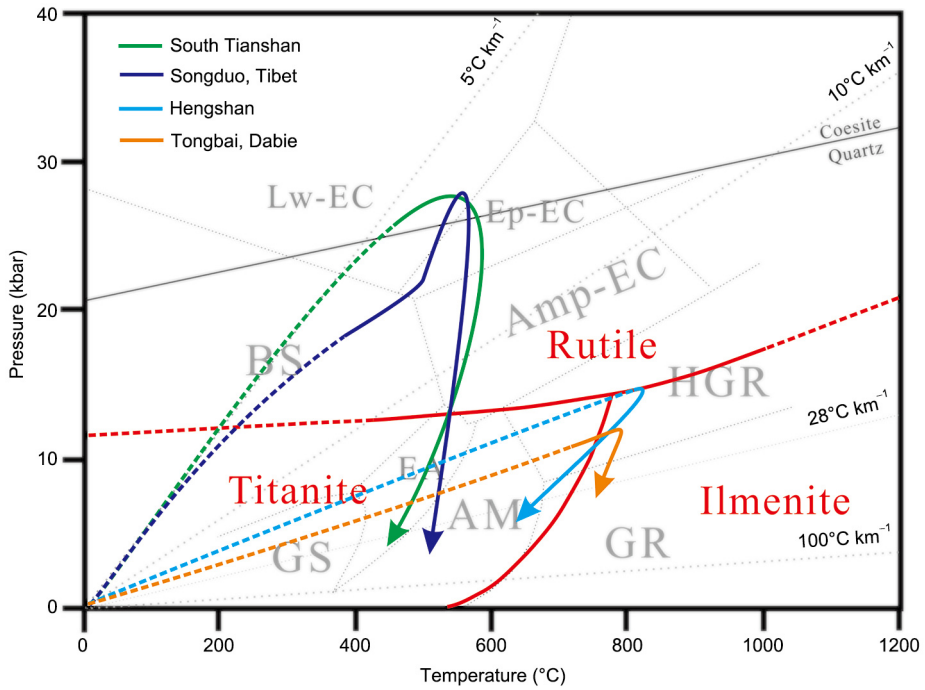


**Figure 6** Metamorphic *P-T* paths of ilmenite- and rutile- bearing metamorphic rocks from different subduction zones. Metamorphic reaction boundaries and abbreviations (dash lines) are from Liou et al., (2004). Phase relations of rutile, titanite and ilmenite in the MORB+$H_2O$ system (red lines) are from Liou et al. (1998).

field at high pressure (>~1.2 GPa), titanite occurs at low *P* (<~1.2 GPa) and *T* (<~600–800°C), and ilmenite is confined to low *P* (<~1.5 GPa) and high *T* (>~600–800°C). Accordingly, rutile is the Ti-bearing phase in the eclogites, and should be fully or partially replaced by ilmenite or titanite during later retrograde process, as demonstrated by the eclogites from the Southwestern Tianshan and Sumdo, Lhasa block of Tibetan Plateau (Figure 5a and b). On the other hand, the coexisting of rutile and ilmenite, as observed in amphibolite from Wutai-Hengshan, North China (Figure 5c) and granulites from Tongbai, Dabie Shan, China (Figure 5d), may represent the prograde metamorphism. It follows that the oxygen fugacity constrained by coexisting rutile and ilmenite in the eclogites may represent only the redox state in the retrograde process (at ~1.5 GPa; Figure 6) whereas that constrained by coexisting rutile and ilmenite in the amphibolites and granulites may represent the redox state of (near) peak metamorphism.

To facilitate a comparison of the redox states of these different metamorphic rocks, it is better to renormalize the $fO_2$ values to the *P-T* conditions of 1.5 GPa and 700°C, which are close to the *P-T* conditions for the coexisting of rutile, ilmenite and titanite (Liou et al., 1998; Figure 6). The compositions of the ilmenite and rutile observed in these metamorphic rocks were obtained by using the electron microprobe at Peking University (Table S2 and Table 3). From these compositional data, the activity of $FeTiO_3$ and $Fe_2O_3$ in the ilmenites, and the activity of $TiO_2$ in the rutiles were calculated as above. The $fO_2$ was subsequently calculated by using the rutile-ilmenite oxybarometer (eq. (3); Zhao et al., 1999) at 1.5 GPa and 700°C. The final results are shown in Table 3. Evidently, all these metamorphic rocks show similar $fO_2$ values (ranging from −15.97 to −14.37), with the two retrograded eclogites are slightly more oxidizing than the amphibolites and granulites (Table 3).

The rutile-ilmenite oxybarometer may be somewhat simplified on the basis of two reasonable assumptions: (1) The activity of $TiO_2$ in rutile is 1; (2) The effects of minor Mg,

**Table 3** $fO_2$ of metamorphic rocks calculated by RI oxybarometer at 1.5 GPa and 700°C

| Location | Rock type | Sample # | Mole fractions | | | | | Activity | | | | | log$fO_2$ | ΔFMQ |
|---|---|---|---|---|---|---|---|---|---|---|---|---|---|---|
| | | | $FeTiO_3$ | $MgTiO_3$ | $MnTiO_3$ | $Fe_2O_3$ | $TiO_2$(Ru) | $Fe_2O_3$ | $FeTiO_3$ | $MgTiO_3$ | $MnTiO_3$ | $TiO_2$ | RI | |
| South Tianshan | Eclogite | A300-9 | 0.915 | 0.001 | 0.035 | 0.038 | 0.983 | 0.065 | 0.894 | 0.002 | 0.022 | 0.983 | −14.718 | 0.644 |
| Songduo, Tibet | Eclogite | SD-30 | 0.919 | 0.009 | 0.002 | 0.038 | 0.994 | 0.107 | 0.948 | 0.016 | 0.001 | 0.994 | −14.368 | 0.994 |
| Hengshan, North China | Amphibole | H1313 | 0.889 | 0.003 | 0.086 | 0.011 | 0.992 | 0.016 | 0.929 | 0.008 | 0.081 | 0.992 | −15.972 | −0.610 |
| Tongbai, Dabie | Granulite | 811133Y | 0.957 | 0.004 | 0.014 | 0.012 | 0.991 | 0.024 | 0.925 | 0.008 | 0.007 | 0.991 | −15.617 | −0.255 |

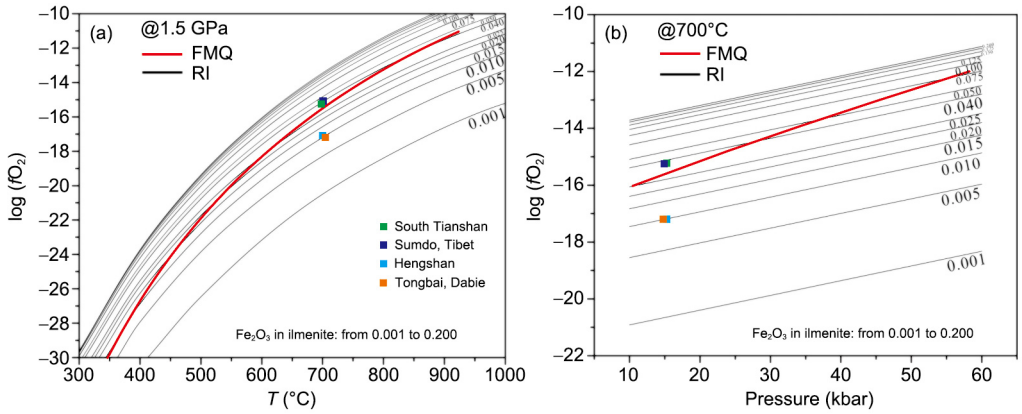


**Figure 7** Log $fO_2$-$T$ diagram of the rutile-ilmenite oxybarometer in the FeO-$Fe_2O_3$-$TiO_2$ system with the $Fe_2O_3$ in ilmenite changing from 0.001 to 0.200. The FMQ buffer (red curve) was calculated by the Thermocalc software (tc336i) with newly updated thermodynamic data (Holland and Powell, 2011).

Mn and Al in the ilmenite are negligible. The ilmenite-rutile oxybarometer then is fully dictated by the $Fe_2O_3$ concentration in the ilmenite, which will be further discussed in this paper. Because there is a miscibility gap along the join hematite-ilmenite and the molar fraction of the $Fe_2O_3$ in the ilmenite mostly does not exceed 0.2 at relative low temperatures (Buddington and Lindsley, 1964; Ghiorso, 1990), we explore the $fO_2$ of the rutile+ilmenite phase assemblage for the $Fe_2O_3$ range of 0.001–0.200 only. The calculated $fO_2$ values are shown in Figure 7a for the pressure of 1.5 GPa, and in Figure 7b for the temperature of 700°C. The $fO_2$ of the FMQ buffer, calculated by using the Thermocalc software (tc336i) with the thermodynamic database of Holland and Powell (2011), is also sketched (red line). As shown in Figure 7, the $fO_2$ of the rutile+ilmenite phase assemblage spans from ~FMQ-4 to ~FMQ+3, which covers the common redox states of the most metamorphic rocks from different subduction zones (Foley, 2011). It follows that the rutile-ilmenite oxybarometer may have a wide application.

There are some prerequisites before using Figure 7 to estimate the $fO_2$ of the metamorphic rocks equilibrated at crust $P$-$T$ conditions: (1) rutile locally equilibrated with ilmenite; (2) molar content of $TiO_2$ in the rutile should be near 100%; (3) negligible Mg, Mn and Al occur in ilmenite; (4) mole fraction of $Fe_2O_3$ in ilmenite should be lower than 0.2. If all of above requirements are met, the $fO_2$ of the metamorphic rocks can be approximated by using Figure 7.

**Acknowledgements** *We thank two reviewers (Dr. Youxue Zhang and an anonymous reviewer) for their constructive suggestions, and Qiang He and Xiaoli Li for their assistance with the instruments used in this study. This work was supported by the National Natural Science Foundation of China (Grant Nos. 41520104004 & 41502038) and the China Postdoctoral Science Foundation (Grant No. 2015M570009).*

## References

Andersen D J, Bishop F C, Lindsley D H. 1991. Internally consistent solution models for Fe-Mg-Mn-Ti oxides: Fe-Mg-Ti oxides and olivine. Am Miner, 76: 427–444

Anovitz L M, Essene E J, Metz G W, Bohlen S R, Westrum Jr. E F, Hemingway B S. 1993. Heat capacity and phase equilibria of almandine, $Fe_3Al_2Si_3O_{12}$. Geochim Cosmochim Acta, 57: 4191–4204

Arculus R J. 1985. Oxidation status of the mantle: Past and present. Annu Rev Earth Planet Sci, 13: 75–95

Bader T, Franz L, De Capitani C, Zhang L. 2014. The effect of water activity on calculated phase equilibria and garnet isopleth thermobarometry of granulites, with particular reference to Tongbai (east-central China). Eur J Mineral, 26: 5–23

Bellis A, Canil D. 2006. Ferric iron in $CaTiO_3$ perovskite as an oxygen barometer for kimberlitic magmas I: Experimental calibration. J Petrol, 48: 219–230

Buddington A F, Lindsley D H. 1964. Iron-titanium oxide minerals and synthetic equivalents. J Petrol, 5: 310–357

Bézos A, Humler E. 2005. The $Fe^{3+}/\Sigma Fe$ ratios of MORB glasses and their implications for mantle melting. Geochim Cosmochim Acta, 69: 711–725

Canil D, Bellis A J. 2007. Ferric iron in $CaTiO_3$ perovskite as an oxygen barometer for kimberlite magmas II: Applications. J Petrol, 48: 231–252

Carmichael I S E, Nicholls J. 1967. Iron-titanium oxides and oxygen fugacities in volcanic rocks. J Geophys Res, 72: 4665–4687

Christie D M, Carmichael I S E, Langmuir C H. 1986. Oxidation states of mid-ocean ridge basalt glasses. Earth Planet Sci Lett, 79: 397–411

Dai L, Hu H, Li H, Jiang J, Hui K. 2014. Influence of temperature, pressure, and chemical composition on the electrical conductivity of granite. Am Miner, 99: 1420–1428

Donohue C L, Essene E J. 2000. An oxygen barometer with the assemblage garnet-epidote. Earth Planet Sci Lett, 181: 459–472

Foley S F. 2011. A reappraisal of redox melting in the Earth's mantle as a function of tectonic setting and time. J Petrol, 52: 1363–1391

French B M, Rosenberg P E. 1965. Siderite ($FeCO_3$): Thermal decomposition in equilibrium with graphite. Science, 147: 1283–1284

Frost B R. 1979a. Metamorphism of iron-formation: Parageneses in the system Fe-Si-C-O-H. Econ Geol, 74: 775–785

Frost B R. 1979b. Mineral equilibria involving mixed-volatiles in a C-O-H fluid phase: The stabilities of graphite and siderite. Am J Sci, 279: 1033–1059

Frost D J, McCammon C A. 2008. The redox state of Earth's mantle. Annu Rev Earth Planet Sci, 36: 389–420

Ghiorso M S. 1990. Thermodynamic properties of hematite-ilmenite-geikielite solid solutions. Contrib Mineral Petrol, 104: 645–667

Ghiorso M S, Evans B W. 2008. Thermodynamics of rhombohedral oxide solid solutions and a revision of the FE-TI two-oxide geothermometer and oxygen-barometer. Am J Sci, 308: 957–1039

He Q, Tang J, Wang F, Liu X. 2014. High Temperature stable assembly

desighed fro cubic press. Chin J High Pressure Phys, 28: 145–151
Holland T J B, Powell R. 2011. An improved and extended internally consistent thermodynamic dataset for phases of petrological interest, involving a new equation of state for solids. J Metamorph Geol, 29: 333–383
Jakobsson S. 2012. Oxygen fugacity control in piston-cylinder experiments. Contrib Mineral Petrol, 164: 397–406
Kelley K A, Cottrell E. 2009. Water and the oxidation state of subduction zone magmas. Science, 325: 605–607
Lee C T A, Luffi P, Le Roux V, Dasgupta R, Albaréde F, Leeman W P. 2010. The redox state of arc mantle using Zn/Fe systematics. Nature, 468: 681–685
Lindsley D H. 1991. Oxide minerals: Petrologic and magnetic significance. Rev Mineral, 25
Liou J G, Zhang R, Ernst W G, Liu J, McLimans R. 1998. Mineral paragenesis in the Pianpaludo eclogitis body, Gruppo di Voltri, western Ligurian Alps. Schweizerische Mineralogische und Petrographische Mitteilungen, 78: 317–335
Liou J G, Tsujimori T, Zhang R Y, Katayama I, Maruyama S. 2004. Global UHP metamorphism and continental subduction/collision: The Himalayan Model. Int Geol Rev, 46: 1–27
Liu X, Chen J, Tang J, He Q, Li S, Peng F, He D, Zhang L, Fei Y. 2012. A large volume cubic press with a pressure-generating capability up to about 10 GPa. High Pressure Res, 104: 1–16
Malaspina N, Poli S, Fumagalli P. 2009. The oxidation state of metasomatized mantle wedge: Insights from C-O-H-bearing garnet peridotite. J Petrol, 50: 1533–1552
Parkinson I J, Arculus R J. 1999. The redox state of subduction zones: Insights from arc-peridotites. Chem Geol, 160: 409–423
Qian J H, Wei C J. 2016. *P-T-t* evolution of garnet amphibolites in the Wutai-Hengshan area, North China Craton: Insights from phase equilibria and geochronology. J Metamorph Geol, 34: 423–446
Ryerson F J, Durham W B, Cherniak D J, Lanford W A. 1989. Oxygen diffusion in olivine: Effect of oxygen fugacity and implications for creep. J Geophys Res, 94: 4105–4118
Tao R, Fei Y, Zhang L. 2013. Experimental determination of siderite stability at high pressure. Am Miner, 98: 1565–1572
Tao R, Zhang L, Fei Y, Liu Q. 2014. The effect of Fe on the stability of dolomite at high pressure: Experimental study and petrological observation in eclogite from southwestern Tianshan, China. Geochim Cosmochim Acta, 143: 253–267
Tian Z L, Wei C J. 2013. Metamorphism of ultrahigh-pressure eclogites from the Kebuerte Valley, South Tianshan, NW China: Phase equilibria and *P-T* path. J Metamorph Geol, 31: 281–300
Whitney D L, Evans B W. 2010. Abbreviations for names of rock-forming minerals. Am Miner, 95: 185–187
Wood B J, Virgo D. 1989. Upper mantle oxidation state: Ferric iron contents of Iherzolite spinels by $^{57}$Fe Mössbauer spectroscopy and resultant oxygen fugacities. Geochim Cosmochim Acta, 53: 1277–1291
Yang X, Zhang L, Zhao Z, Zhu D. 2014. Metamorphic evolution of glaucophane eclogites from Sumdo, Lhasa block of Tibeteau: Phase equilibra and metamorphic *P-T* path. Acta Petrol Sin, 30: 1505–1519
Zhao D G, Essene E J, Zhang Y X. 1999. An oxygen barometer for rutile-ilmenite assemblages: Oxidation state of metasomatic agents in the mantle. Earth Planet Sci Lett, 166: 127–137